THE JOURNAL OF PHYSICAL CHEMISTRY B

Article

pubs.acs.org/JPCB

Conductivity and Spectroscopic Investigation of Bis(trifluoromethanesulfonyl)imide Solution in Ionic Liquid 1-Butyl-3-methylimidazolium Bis(trifluoromethanesulfonyl)imide

Lei Yu,* Benjamin S. Pizio, and Timothy D. Vaden*

Department of Chemistry and Biochemistry, Rowan University, Glassboro, New Jersey 08028, United States

ABSTRACT: Protic ionic liquids (PILs) are promising alternatives to water for swelling Nafion as a fuel cell proton exchange membrane (PEM). PILs can significantly improve the high-temperature performance of a PEM. The proton dissociation and solvation mechanisms in a PIL, which are keys to understanding the proton transportation and conductivity, have not been fully explored. In this paper, we used FTIR, Raman, and electronic spectroscopy with computational simulation techniques to explore the spectroscopic properties of bis(trifluoromethanesulfonyl)imide (HTFSI) solutions in 1-butyl-3-methylimidazolium bis(trifluoromethanesulfonyl)imide (BMITFSI) ionic liquid at concentrations from ∼0.1 to as high as ∼1.0 M. Solution conductivities were measured at room temperature and elevated temperatures up to ∼65 °C. The solution structure and properties depend on the concentration of HTFSI. At lower concentration, around 0.1 M, the HTFSI solution has higher conductivity than pure BMITFSI. However, the conductivity decreases when the concentration increases from 0.1 to 1.0 M. Temperature-dependent conductivities followed the Vogel−Fulcher−Tamman equation at all concentrations. Conductivity and spectroscopy results elucidate the complicated ionization and solvation mechanism of HTFSI in BMITFSI solutions. Raman spectroscopy and density functional theory (DFT) calculations are consistent with the complete ionization of HTFSI to generate solvated H^+ at low concentrations. FTIR, Raman, and electronic spectroscopic results as well as DFT computational simulation indicated that when the concentration is as high as 1.0 M, a significant amount of $TFSI^-$ is protonated, most likely at the imide nitrogen.

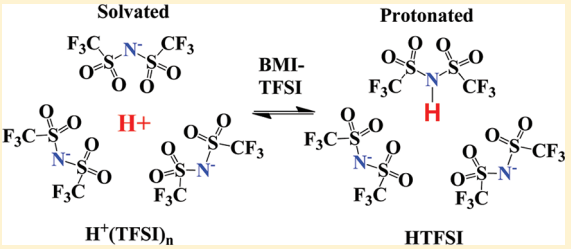

INTRODUCTION

Room-temperature ionic liquids (ILs) have recently become a focus of scientific interest due to their remarkable properties, such as negligible vapor pressures, low melting points, nonflammability, good solvation of many organic and inorganic chemicals, and high ionic conductivities.[1] These properties make ILs advanced candidates for numerous applications, including as both solvents and electrolytes for electrochemical processes such as those used in fuel cells, lithium batteries, and solar cells.[2−25] ILs offer excellent high-temperature performance, a long life, and safety as a result of their negligible volatility, thermostability, and nonflammability.

Fuel cells receive significant attention in chemistry and engineering for several reasons. Fuel cells can produce a continuous electric charge as long as fuels are supplied. Currently, fuel cells can be used as both low- and high-power energy supplies for portable electronic devices and domestic appliances, as well as automobiles and airplanes. Fuels such as hydrogen, oxygen, and methanol are in high natural abundance, and their products are "green" to the environment. Currently, devices based on the proton exchange membrane (PEM) are the dominant fuel cell variety. In a PEM fuel cell, protons produced at the anode transfer through the PEM to the cathode. The rate, selectivity, nondestructiveness, and completeness of this proton transfer determine the overall performance of a fuel cell. Nafion, a perfluorosulfonic acid membrane, is widely used in PEM fuel cells due to its excellent thermal and chemical stability, proton conductivity, and mechanical strength.[26−30] Nafion provides high proton conductivity only when it is fully hydrated. At temperatures close to or above 100 °C, fast water evaporation results in significant reduction of proton conductivity, usually ending in cell failure. However, working at around 100−150 °C is desirable because higher temperature reduces the catalyst poisoning and increases fuel cell efficiency.[31]

Using IL-containing polymer membranes as the PEM of fuel cells may solve the aforementioned problems associated with hydrated Nafion. For example, polymer gel electrolyte containing the IL 1-butyl-3-methylimidazolium triflate ($BMICF_3SO_3$) and 1-butyl-3-methylimidazolium tetrafluoroborate ($BMIBF_4$) exhibits high ionic conductivity ($\sim 10^{-2}-10^{-1}$ S/cm) at around 200 °C.[32] Their low volatilities and high thermostabilities allow IL-based PEMs to be heated to a temperature as high as ∼300 °C without observable IL evaporation and loss of electrochemical functionality. To obtain high proton conductivity, protic ionic liquids (PILs) have been developed and used as PEM components.[16−22] A PIL is a Brønsted acid−base combination of an anion and

Received: February 26, 2012
Revised: May 13, 2012

   dx.doi.org/10.1021/jp301883e | J. Phys. Chem. B XXXX, XXX, XXX−XXX

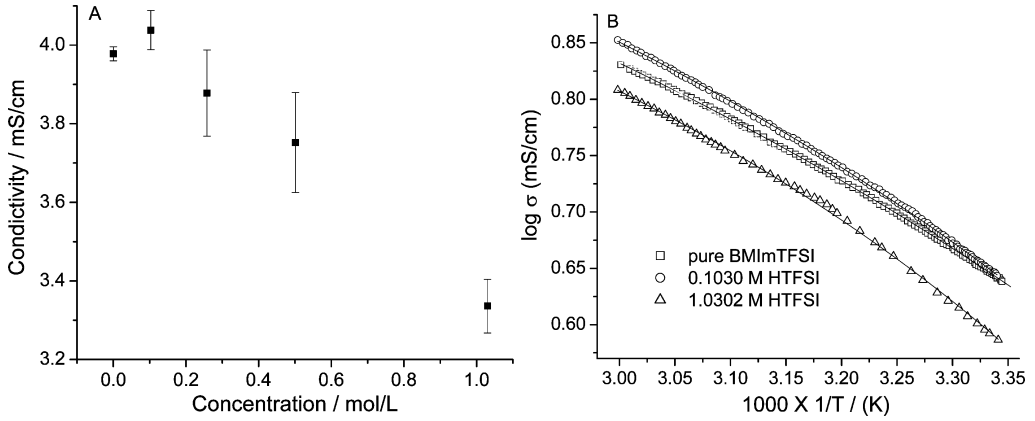

Figure 1. (A) Conductivity vs HTFSI concentration in BMITFSI solutions at 23 °C. (B) Arrhenius plots (conductivity vs temperature) of pure BMITFSI (□), 0.1030 M HTFIS (○), and 1.0302 M HTFSI (△).

cation in which proton transfer from acid to base creates two molecular ions.[33] PILs swelled into Nafion polymer membranes are the proton sources for hydrogen bonding and proton conductivity within the composite. Indeed, the PIL ethylammonium nitrate (EAN) has many functional similarities to water.[33,34] In PIL electrolytes, the proton transport mechanism may depend on cation/anion structures, the PIL physicochemical properties, and the abundance of "extra" protons. In this latter context, a proton may be associated (solvated) with multiple anions to form a negatively charged cluster.[35] The proton may be transported by molecular carriers such as protonated cations or anions.[36] Proton hopping could also occur between the proton donor and acceptor in amine-containing PILs.[37] The existence of an appreciable concentration of contaminations such as water (0.1%, w/w) can affect the mechanism of proton transportation and the conductivity of the proton.[38]

To achieve high proton conductivity, a high proton concentration is essential. Addition of a Brønsted acid can directly increase the acidic proton in an IL solution. So far, an optimal Brønsted acid that can make a proton-rich IL solution is not available. Several potential Brønsted acids such as EAN, hydrogen sulfate (RSO_3H), trifluoroacidic acid (TFA), and, relevant to the current work, bis(trifluoromethanesulfonyl)-imide (HTFSI) have been considered and investigated.[33,37] The self-dissociation of HTFSI produces "free" protons that can immediately be solvated by the anions in the solution. Dissociation also produces the TFSI anion present in many ILs. These dissociation and solvation mechanisms are the keys to understanding proton transportation and conductivity, which has not been fully explored.

The solution structure of a proton solvated in an IL is a key unknown in understanding the solvation process. Protons may be solvated with only one anion to form an ion pair, may be solvated by multiple anions to make an ion cluster, or may bind covalently to form a protonated molecule.[37] Vibrational spectroscopic methods are a powerful means for the investigation of the solvation process and molecular interactions, including the interactions of ILs with other molecules.[39−41] The spectral peaks in IL molecules are significantly affected by the interactions of protons and other IL molecules. Raman and infrared spectroscopy (FTIR) together can offer complementary vibrational spectroscopic information. Proton-solvation structures can also be investigated by computational simulation using the "miniclusters" method of Angenendt and Johansson.[9] Structural predictions, with observations from vibrational spectroscopy, can help explain the results of the conductivity experiments. In this paper, we use these techniques to explore the conductivity and spectroscopic properties of HTFSI solutions in IL 1-butyl-3-methylimidazolium bis(trifluoromethanesulfonyl)imide (BMITFSI) at concentrations from ∼0.1 to as high as ∼1.0 M.

EXPERIMENTAL SECTION

Chemicals. The IL BMITFSI (>97% pure) was purchased from EMD Chemicals Inc. It was dried in a vacuum oven overnight at 60 °C prior to use. LiTFSI (>99% pure) and HTFSI (>95% pure) were purchased from Fluka and were used as received. All other chemicals were purchased from Sigma-Aldrich and used as received. Concentrated (∼1.0 M) HTFSI and LiTFSI solutions in BMITFSI were prepared first; lower concentration solutions were prepared by dilution with BMITFSI solvent from the concentrated solutions.

Ionic Conductivity. The conductivities of pure ILs and IL solutions were measured by an AC Mode Traceable conductivity meter at a constant frequency of 3 kHz with a pair of parallel Pt plate electrodes. The cell constant is designed to be unity. The temperature (between ∼20 and 80 °C) of the IL solutions was controlled by a hot-water bath and monitored by a built-in thermal couple of the conductivity probe.

Spectroscopy and Density Functional Theory (DFT) Simulation. FTIR spectra were measured with a Varian FTS 7000 FTIR spectrometer at 1 cm^{-1} resolution with a KBr pellet for solid samples and a TlBrI salt plate for liquid samples. Electronic spectra were measured with an HP 1100 UV−vis spectrometer at room temperature with pure BMITFSI as the background. Raman spectra were measured using a 17 mW HeNe laser source at 633 nm. Raman-scattered photons were detected and analyzed with a Horiba Jobin-Yvon microHR grating spectrometer with a 50 μm slit entrance. The detector was an Andor Newton charge coupled device (CCD) camera, and the instrument resolution was around 10 cm^{-1}. Each spectrum was generated by averaging ∼15 individual scans, each corrected for background using standard baseline-adjustment software.

DFT simulation of IL solvation structures was performed with the Schrodinger suite of programs (Schrodinger, Inc.). Miniclusters of several IL units were modeled with molecular mechanics (MM) and DFT quantum chemical calculations. For the pure BMITFSI IL, two BMI (1-butyl-3-methylimidazolium)

dx.doi.org/10.1021/jp301883e | J. Phys. Chem. B XXXX, XXX, XXX−XXX

and two bis(trifluoromethanesulfonyl)imide molecules were used to build a minicluster; for HTFSI−BMITFSI solution, a H^+ and an additional $TFSI^-$ ion were added. For each species calculated, a comprehensive MM conformational search was performed with the OPLS-2005 force field. Geometries and vibrational frequencies of selected low-energy conformations were computed with DFT calculations using the M05-2X functional (chosen to treat dispersion) and the 6-31+G* basis set. The unscaled frequencies were used to compute absolute free energies for each structure at 298 K.

RESULTS AND DISCUSSION

Conductivity Results. The conductivity of HTFSI solutions in BMITFSI was measured and is shown in Figure 1. The 0.1030 M HTFSI solution has a slightly higher conductivity relative to pure BMITFSI. Conductivity values decreased gradually as the HTFSI concentration increased from 0.1030 to 1.0302 M. Previous reports[15,42] have demonstrated that the LiTFSI and NaTFSI solution conductivity decreases approximately proportionally with increasing metal cation concentration. Compared to the mean values and the standard deviations, this increment may or may not be statistically significant. However, the conductivity clearly behaves differently from that of the the Li^+ and Na^+ solutions,[15,42] as it may slightly increase and does not decrease until concentrations higher than 0.15 M. At elevated temperatures (25−65 °C), similar results were obtained: The conductivity increased at lower HTFSI concentration and decreased at higher HTFSI concentration. Furthermore, this trend was also observed at higher temperatures. Figure 1B shows conductivity Arrhenius plots for both pure BMITFSI and HTFSI−BMITFSI solutions. Concurrent with previous reports of IL-based solution conductitivies,[37,43,44] the conductivity Arrhenius plots are not straight lines, but rather curves that fit the Vogel−Fulcher−Tamman (VFT) equation:

$$\sigma = \sigma_0 \exp\left[-\frac{B}{T - T_0}\right] \tag{1}$$

where σ_0, B, and T_0 are constants for a system, which have been described in the free-volume theory.[43] Their values vary in different liquids or solutions. The values of these constants were obtained by fitting the experimental data with the VFT equation and are summarized in Table 1.

Table 1. VFT Equation Parameters Obtained by Fitting the Experimental Data in Figure 1B

	σ_0 (mS/cm)	B (K)	T_0 (K)
pure BMITFSI	27.7 ± 0.7	201 ± 5.8	190 ± 1.8
0.1030 M HTFSI	26.6 ± 0.8	169 ± 6.5	205 ± 2.1
1.0302 M TFSI	19.4 ± 0.7	112 ± 7.0	225 ± 2.6

To understand the conductivity results, we investigated the nature of HTFSI in aqueous and IL solutions. Experimental results (not shown) indicate that HTFSI is a typical Brønsted strong monoprotic acid in aqueous solutions. For example, a 0.1 M aqueous solution of HTFSI has pH close to 1.0. This solution can be titrated by both strong and weak Brønsted bases, yielding typical titration curves. In IL solutions, HTFSI has also been reported to be a monoprotic Brønsted acid and, therefore, a possible proton source for imidazole- and pyrazole-based proton-conducting materials.[37,45] The acidic strength (pK_a) of HTFSI in ILs is unknown, but it is likely a stronger acid than imidazolium as facile proton transfer from HTFSI to imidazole has been observed.[37] Once HTFSI dissolves in BMITFSI, the following reaction system involving dissociation, solvation, and waterlike autoionization could exist at equilibrium:

$$\text{dissociation:}\quad \mathrm{HTFSI} \rightarrow \mathrm{H^+} + \mathrm{TFSI^-} \tag{2}$$

$$\text{solvation:}\quad \mathrm{H^+} + n\mathrm{TFSI^-} \rightarrow [\mathrm{H(TFSI)}_n]^{(n-1)-} \quad (n = 2 \text{ or } 3) \tag{3}$$

$$\text{autoionization:}\quad 2\mathrm{HTFSI} \rightarrow \mathrm{TFSI^-} + [\mathrm{H_2TFSI}]^+ \tag{4}$$

These reactions will necessarily affect proton conductivity in an IL solution. The conductivity (σ) of an electrolyte solution can be described by the equation:

$$\sigma = F \sum_i Z_i C_i b_i \tag{5}$$

where F is Faraday's constant, Z_i is the charge of one ion, C_i is the concentration of the ion, and b_i is the mobility of the ion. According to eq 5, either changing the ion concentration or changing the ion mobility can affect the overall conductivity of a solution. Ionization and solvation processes may affect the overall conductivity of the solution in several ways. Equations 2−4 could create new charge carriers (ions) in the solution, such as H^+, $[H(TFSI)_n]^{(n-1)-}$, or $[H_2TFSI]^+$. The molar concentration of each ion or the total ion concentration could also change. These changes can affect the viscosity of the solution and the molar conductivity (or mobility) of each ion. The addition of new ions may also change the mechanism of proton conductivity, from pure diffusion of proton carriers to intermolecular proton transfer. These changes that can affect solution conductivity may exist in a solution either individually or simultaneously. For example, in a Li^+ or Na^+ solution in BMITFSI, the solvation of Li^+ or Na^+ and the increase of solution viscosity cause the solution conductivity to decrease gradually with the increase of the Li^+ or Na^+ concentration.[4,9,15,46,47]

In the HTFSI solution, it can be speculated that two different mechanisms may be dominant at low (0.1 M or lower) and high (greater than 0.1 M) concentrations. A maximum conductivity can be observed at about 0.1 M HTFSI (Figure 1A). This observation is consistent with the conductivity profile of an HTFSI/imidazole mixture and H_2SO_4 solutions.[37,45] At lower concentration, the HTFSI may completely or almost completely dissociate or self-ionize, which may increase the overall ion concentration in the IL or produce ions with higher ion mobility. At higher HTFSI concentration, HTFSI may ionize only partially, with an appreciable portion of the HTFSI existing in solution as neutral HTFSI molecules. Incomplete ionization may reduce the ion concentrations or hinder ion transportation, hence yielding a lower conductivity.

FTIR Spectroscopic Results. We measured FTIR spectra for HTFSI−BMITFSI solutions to corroborate the conductivity measurements with structural information. The presence and absence of HTFSI species in the solution can also be reflected by the change of peak intensities in the FTIR spectra, shown in Figure 2. Figure 2A shows FTIR spectra of BMITFSI and its HTFSI solutions with various concentrations from 0.1030 to 1.0302 M. The relative intensities of peaks at 883 and 1437 cm^{-1} increase gradually with increasing HTFSI concentration,

dx.doi.org/10.1021/jp301883e | J. Phys. Chem. B XXXX, XXX, XXX−XXX

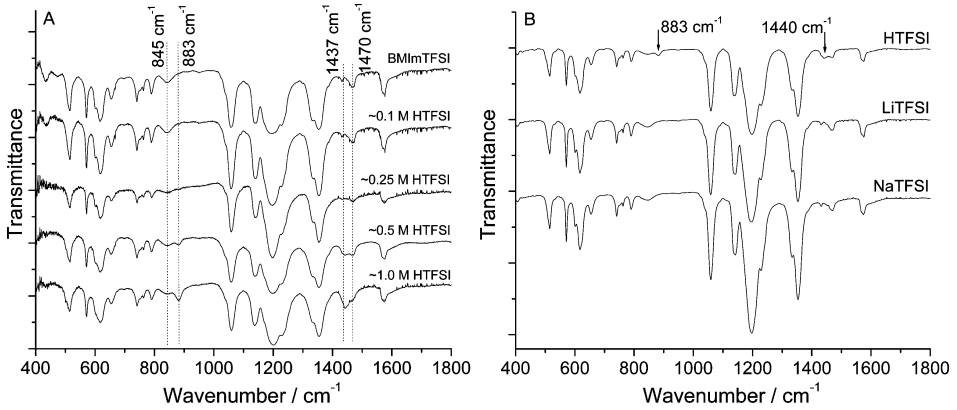

Figure 2. (A) FTIR spectra of BMITFSI and its HTFSI solutions with increasing concentration, from top to bottom, 0.1030, 0.2576, 0.5015, and 1.0302 M. (B) FTIR spectra of NaTFSI, LiTFSI, and HTFSI solutions in BMITFSI.

while peak intensities at 845 and 1470 cm^{-1} remain constant. Notably, the peak at 883 cm^{-1} is not observable and the peak at 1437 cm^{-1} is very weak in the spectra of pure BMITFSI or 0.1030 M HTFSI solution. These peaks correspond to bending and wagging vibrational modes, which have inherently lower IR intensities compared to stretching vibrational modes. However, subtraction of the IR spectra (not shown) confirms that the appearance and subsequent increase of the 883 and 1437 cm^{-1} peaks are significant. In spectra of LiTFSI and NaTFSI solutions (Figure 2B), the 883 cm^{-1} peak is not observed at any concentration and the 1437 cm^{-1} peak is as weak as in the pure BMITFSI spectrum (Figure 2A).

As BMITFSI, NaTFSI, LiTFSI, and HTFSI share the same anion ($TFSI^-$), the two peaks special to the HTFSI solutions likely arise from vibrations of protonated $TFSI^-$. Interestingly, these two peaks can only be observed in IL solutions. FTIR spectra of solid HTFSI, NaTFSI, and LiTFSI (in KBr) do not exhibit these peaks, as shown in Figure 3. We therefore speculate that protonated $TFSI^-$ in solution has a structure different from that of HTFSI in its solid state.

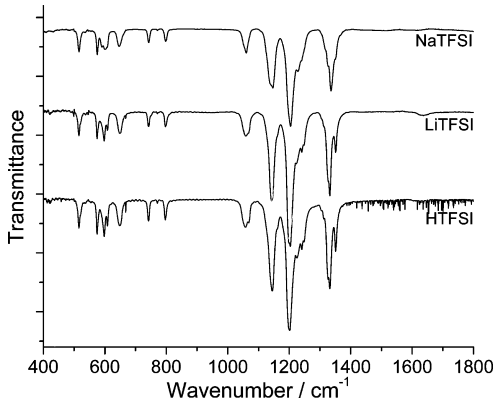

Figure 3. FTIR spectra of solid HTFSI, LiTFSI, and NaTFSI in a KBr pellet.

Raman Spectroscopic Results. The power of vibrational spectroscopy for investigation of IL solution structures is due in part to the sensitivity of molecular vibrations to their solvation environment. The FTIR spectra yield structural clues to understanding the proton conductivity in BMITFSI IL solution, but IL molecular vibrational frequencies do not appear to change significantly with changing concentrations. For further information, we turn to Raman scattering as a complementary vibrational spectroscopic tool. Figure 4 shows the laser-Raman

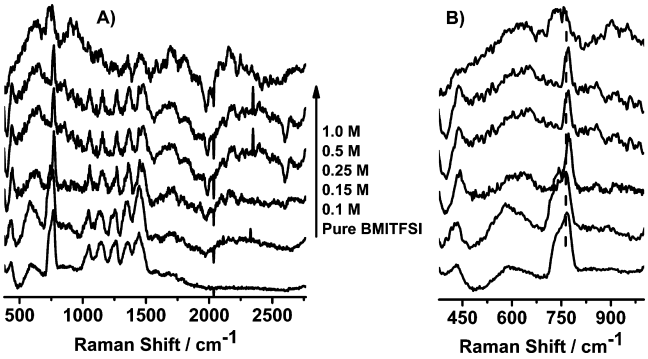

Figure 4. (A) Raman spectra of HTFSI in BMITFSI at different concentrations. (B) Expanded view of the region encompassing the $-CF_3$ umbrella/$-SO_2N-$ umbrella $TFSI^-$ vibration.

spectra of BMITFSI with increasing HTFSI concentration. As the HTFSI concentration increased from 0.1030 to 1.0302 M, the signal-to-noise level decreased because of the increase of background fluorescence (subtracted during data analysis). Raman spectra of ILs and Li^+ solvation in ILs have been reported and discussed in several publications.[46,48,49] In solutions, the Raman spectrum of IL BMITFSI exhibits complex changes with high solute concentration, especially with Li^+. This appears to be the case here as well: Many spectroscopic changes occur as the HTFSI concentration increases in Figure 4A. For example, at 1.0 M, an intense Raman peak at 900 cm^{-1} is detected. A detailed Raman spectroscopic analysis is beyond the scope of this work, and thus, in this paper, we focus our analysis on the vibrational band centered around 800 cm^{-1} (region expanded in Figure 4B). This band corresponds to the $-CF_3$ umbrella/$-SO_2N-$ umbrella vibration of the $TFSI^-$ molecule, as predicted by the DFT calculations and consistent with previous reports.[46,48,49]

From Figure 4B, the CF_3 band clearly shifts to higher wavenumber from the pure BMITFSI up to HTFSI concentrations around 0.15 M. Concurrently, the band evolves from an asymmetric band consisting of two peaks to a single sharp symmetric peak. At an HTFSI concentration of 0.25 M and above, the band further evolves back into an asymmetric shape with two peaks and shifts back to lower wavenumber.

dx.doi.org/10.1021/jp301883e | J. Phys. Chem. B XXXX, XXX, XXX–XXX

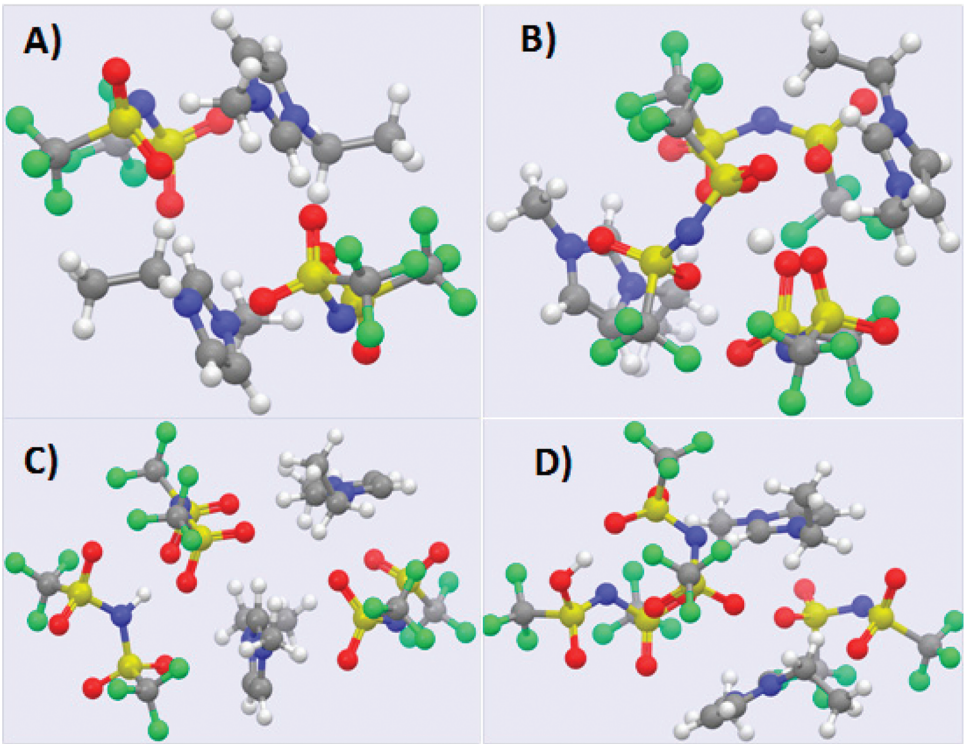

Figure 5. DFT structures of IL miniclusters: (A) pure BMITFSI, comprised of two BMI^+ and two $TFSI^-$ molecules, (B) HTFSI–BMITFSI structure in which the H^+ is solvated by $TFSI^-$, (C) HTFSI–BMITFSI structure in which the $TFSI^-$ is protonated at the nitrogen, (D) HTFSI–BMITFSI structure in which the $TFSI^-$ is protonated at the oxygen. The relative energies of (B)–(D) are stated in the text.

Notably, this concentration-dependent trend, in which the CF_3 band shifts into a sharper, higher wavenumber peak and then back into a broader, lower wavenumber peak, exactly follows the conductivity vs concentration curve in Figure 1. Thus, the Raman spectra are consistent with the conductivity results in that they both predict that the IL structure changes from 0 to 0.15 M and then evolves differently at higher concentrations. It is very likely that these two trends are related; the structural changes in the $TFSI^-$ ions responsible for the trend in Figure 4B are related to the conductivity changes in Figure 1A.

DFT Results. We turn to the DFT simulation for further structural insights. Three different structures for the HTFSI–BMITFSI solution were considered as inputs to the conformational searches (see the Experimental Section), and the final, lowest energy DFT structures for each input are shown in Figure 5. In Figure 5B, the H^+ is not bound covalently to any IL solvent molecule, but rather coordinated to $TFSI^-$ sulfonyl oxygen groups, whereas in Figure 5C,D, the H^+ covalently protonates $TFSI^-$ molecules. From the computed free energies, the protonated structures in Figure 5C,D are more favorable than the free-proton structure (Figure 5B) by 125 kJ/mol. As the miniclusters represent high-concentration solutions, the DFT results clearly predict $TFSI^-$ protonation at high concentration. Unfortunately, miniclusters that represent low-concentration solutions would be prohibitively large for DFT calculation. The DFT results also predict that imide protonation is more favorable than sulfonyl protonation by 36 kJ/mol. These gas-phase DFT results would likely be perturbed by room-temperature dynamics effects, extended solvation, and liquid-phase network effects, etc. A complete theoretical picture would likely be only obtained from a comprehensive molecular dynamics investigation. However, the DFT structures yield clues to the structural motifs for the H^+ solvation in BMITFSI ionic liquid.

The DFT frequency analyses for the structures in Figure 5 are summarized in Table 2. We focus the analysis on a few vibrational modes that can diagnose structural information as inferred from Figures 3 and 4. All reported vibrational wavenumbers are scaled by 0.97 from harmonic values. The pure BMITFSI minicluster exhibits three sets of vibrations that can be confirmed experimentally from Figures 3 and 4. These are the CH bend and wag vibrations on the BMI^+ molecule and the CF_3 umbrella bending vibration on the $TFSI^-$ molecule. These vibrations are present in all four miniclusters from Figure 5 and confirmed in all molecules in Figures 3 and 4. The $TFSI^-$ CF_3 vibrations are predicted to shift to higher wavenumber when the solvated (free) H^+ is added to the minicluster. In the covalently protonated structures, there are two different CF_3 vibrational wavenumbers: one for the HTFSI and one for the $TFSI^-$. The average of these CF_3 vibrations is intermediate in wavenumber between those of the pure BMITFSI and solvated H^+ BMITFSI (although closer in value to that of the free-proton structure). As the concentration-dependent Raman spectral experiments show that the CF_3 vibration shifts up in wavenumber and then back down (into two resolvable bands) at high concentrations, the DFT calculations appear to be consistent with the free-proton structure present at low concentration and protonated HTFSI at high concentration.

Discussion. From the FTIR spectra (Figure 3), we can identify IR vibrations present in all species at 845 and 1470 cm^{-1}, as well as vibrations that appear with increasing HTFSI concentration at 883 and 1437 cm^{-1}. Turning to Table 2, we can identify these high-concentration-specific vibrations. They agree most closely with the NH^+ bending (1436 cm^{-1}) and NH^+ wagging (897 cm^{-1}) modes of the imide-protonated

dx.doi.org/10.1021/jp301883e | J. Phys. Chem. B XXXX, XXX, XXX–XXX

Table 2. Selected Vibrations Predicted from DFT Calculations: Mode Assignment, Wavenumber,[a] and IR Intensity[b]

minicluster	mode	peak (cm^{-1})	intensity (km/mol)	obsd wavenumber (cm^{-1})
pure BMITFSI[c]	BMI CH bend	1486	23	1470 (Figure 3)
	BMI CH wag	861	4	845 (Figure 3)
	TFSI CF_3 bend	762	1	~745–768 (Figure 4)
free-proton HTFSI–BMITFSI[d]	BMI CH bend	1492	21	1470 (Figure 3)
	BMI CH wag	853	66	
	TFSI CF_3 bend	769	2	777 (Figure 4)
imide-protonated HTFSI–BMITFSI[e]	BMI CH bend	1486	23	
	HTFSI NH^+ bend	1436	129	1437 (Figure 3)
	HTFSI NH^+ wag	897	422	883 (Figure 3)
		847	28	845 (Figure 3)
	TFSI CF_3 bend	770	1	761 (Figure 4)
	HTFSI CF_3 bend	762	2	736 (Figure 4)
sulfonyl-protonated HTFSI–BMITFSI[f]	BMI CH-bend	1487	26	
	HTFSI OH^+ bend	1333	228	not observed
	HTFSI OH^+ wag	946	174	not observed
	BMI CH wag	860	1	
	TFSI CF_3 bend	768	7	
	HTFSI CF_3 bend	764	3	

[a]Harmonic DFT frequencies were scaled by 0.97. [b]Raman intensities could not be computed. [c]Figure 5A. [d]Figure 5B. [e]Figure 5C. [f]Figure 5D.

HTFSI molecule. This strongly suggests the experimental presence of such a protonated HTFSI molecule at high concentration. Furthermore, the two intense OH^+ vibrational modes (bending at 1333 cm^{-1} and wagging at 946 cm^{-1}) predicted for the sulfonyl-protonated HTFSI are clearly absent from the FTIR spectra in Figure 3. As the DFT free energies predict that the imide-protonated structure is most favorable (under the high-concentration conditions of the miniclusters), the DFT and FTIR evidence clearly supports the identification of imide-protonated HTFSI as the high-concentration form of the IL solution.

While we were unable to compute Raman spectra, the IR spectra predicted from the DFT calculations can be used to identify structural features from the FTIR spectra in Figure 2. The predicted IR spectra are compared with the experimental spectra in Figure 6. The IR spectrum predicted from the pure BMITFSI structure in Figure 5A (using harmonic frequencies scaled by 0.97 to generate a spectrum with 10 cm^{-1} fwhm Lorentzian profiles) is compared to the pure IL spectrum in Figure 6A. The agreement is excellent, given the inherent inaccuracies in DFT calculations. Notably, the theory

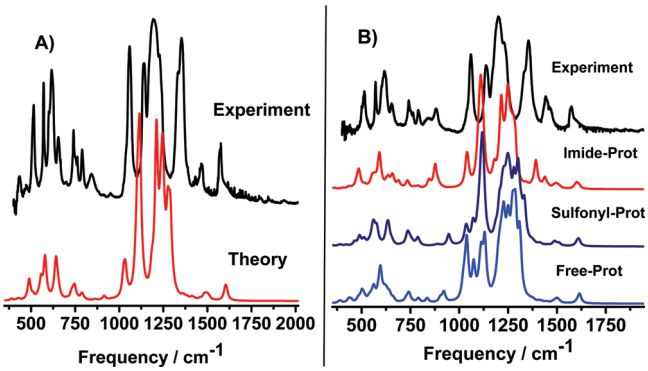

Figure 6. Comparison between experimental and theoretical IR spectra. Harmonic DFT frequencies were scaled by 0.97 and used to generate theoretical spectra with Lorentzian profiles of 10 cm^{-1} width (fwhm). (A) The experimental spectrum (top) for pure BMITFSI is compared to the theoretical spectrum for the pure BMITFSI cluster from Figure 5A. (B) The 1.0 M HTFSI in BMITFSI spectrum is compared to spectra predicted for imide-protonated BMITFSI (from Figure 5C), sulfonyl-protonated BMITFSI (from Figure 5D), and free-proton IL (from Figure 5B).

reproduces the peaks at 1470 and 843 cm^{-1} (and 1550 cm^{-1}, although it has not been discussed) very well. The experimental spectrum for the IL solution with 1.0 M HTFSI is analyzed with the theoretical high-concentration DFT structures from Figure 5 in Figure 6B. Importantly, only the imide-protonated HTFSI–BMITFSI structure (Figure 5C) agrees with the experiment. Only this structure correctly predicts the experimental IR peaks at 883 and 1437 cm^{-1}. This confirms the existence of the imide-protonated structural motif at high H^+ concentration.

Combining all of our results, we speculate that, at lower and higher concentrations, the solvation models of H^+ are different. In pure BMITFSI, both *trans*- and *cis*-$TFSI^-$ exist. The standard Gibbs free energy difference between *trans*- and *cis*-$TFSI^-$ is reported to be as small as 0.2 kJ/mol.[41] At lower concentration, the dissociated protons are solvated by, thermal dynamically preferable, several (2–3) *cis*-$TFSI^-$ ions, Figure 5B. To form a solvation cluster, the *trans*-$TFSI^-$ in the bulk BMITFSI converts to *cis*-$TFSI^-$. DFT free energies of the *trans*-$TFSI^-$ version of Figure 5B (not shown) are unfavorable (relative to the *all-cis* version) by more than 25 kJ/mol. When the concentration of the H^+ is high enough, above 0.25 M, for example, the majority of the $TFSI^-$ ions are within the solvation "cloud" of H^+ ions. Further increasing the HTFSI concentration results in protonation at the imide nitrogen of $TFSI^-$. The free-proton solvated H^+ structure is at best a minor player at high concentration.

Both HTFSI and BMITFSI are colorless. However, HTFSI solution in BMITFSI shows a pink color. Turning to electronic spectroscopy (Figure 7), BMITFSI has an absorption band at about 275 nm, Figure 7A. The electronic spectrum of HTFSI in IL solution is shown in Figure 7B. The 275 nm absorption shifts to either 256 or 306 nm and leaves a negative peak at 285 nm because BMITFSI was used as the background. Meanwhile, two additional peaks at 378 and 499 nm appear in Figure 7B and increase in intensity with increasing HTFSI concentration. The peak at 499 nm explains the pink color of the HTFSI IL solution. This peak was observed only in HTFSI solution in BMITFSI and is absent in the spectra of HTFSI in water, HTFSI in $BMIBF_4$, LiTFSI in BMITFSI, and NaTFSI in

dx.doi.org/10.1021/jp301883e | J. Phys. Chem. B XXXX, XXX, XXX–XXX

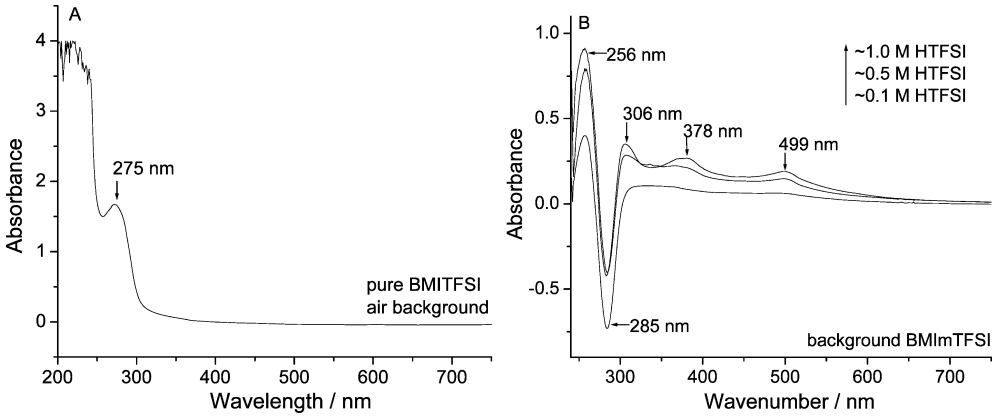

Figure 7. UV−vis spectra of BMITFSI (A) and HTFSI (B) solutions with various concentrations. Pure BMITFSI was used as the background for (B).

BMITFSI (results not shown). These peaks may arise from the imide-protonated HTFSI (not present in aqueous solutions of HTFSI due to complete dissociation), perhaps from a $\pi \rightarrow \pi^*$ excitation.

Taken together, our results strongly suggest that, in HTFSI−BMITFSI IL solutions at low concentrations, the H^+ is free and solvated by the $TFSI^-$ sulfonyl groups. At higher concentrations, the $TFSI^-$ becomes protonated at the imide nitrogen. These solvation and protonation phenomena clearly affect the IL solution conductivities. When the H^+ is solvated, it can act as a charge carrier, and therefore, the solution conductivity is increased relative to that of the pure IL solvent. However, the protonation at high solute concentration acts to degrade the conductivity of the IL system, with clear ramifications for the use and applicability of such solutions in technology.

CONCLUSIONS

Conductivity and spectroscopy results elucidate the complicated ionization and solvation mechanism of HTFSI in BMITFSI solutions. The solution structure and properties depend on the concentration of HTFSI. At lower concentration, around 0.1 M, the HTFSI solution has higher conductivity than pure BMITFSI. However, the conductivity decreases when the concentration increases from 0.1 to 1.0 M. This phenomenon was not observed in Li^+ and Na^+ solutions, which indicates the special nature of H^+ in the BMITFSI solution. Raman spectroscopy and DFT calculations are consistent with the complete ionization of HTFSI to generate solvated H^+ at low concentration. The overall effect of this ionization is to incrementally increase the solution ionic conductivity. The addition of a proton to the solution affects the conformation of $TFSI^-$ in the solution, which comes from both HTFSI and BMITFSI. In the neat (or bulk) BMITFSI, both *trans*- and *cis*-$TFSI^-$ isomers exist, but when $TFSI^-$ solvates protons in solution, the $TFSI^-$ is confined to the *cis*-conformation. As the HTFSI concentration increases, $TFSI^-$ ions in solution are either involved in the solvation of H^+ or protonated. When the concentration is as high as 1.0 M, a significant amount of $TFSI^-$ is protonated, most likely at the imide nitrogen. These changes at the molecular level can be reflected by the FTIR, Raman, and UV−vis spectroscopic results as well as DFT computational simulation.

AUTHOR INFORMATION

Corresponding Author

*Phone: (856) 256-5409 (L.Y.); (856) 256-5457 (T.D.V.). Fax: (856) 256-4478 (L.Y.); (856) 256-4478 (T.D.V.). E-mail: yu@rowan.edu (L.Y.); vadent@rowan.edu (T.D.V.).

Notes

The authors declare no competing financial interest.

ACKNOWLEDGMENTS

T.D.V. acknowledges James Lisy for providing a HeNe laser for preliminary experiments. This work is supported by Rowan University.

REFERENCES

(1) Wasserscheid, P.; Welton, T. *Ionic Liquids in Synthesis*, 2nd ed.; Wiley-VCH: Weinheim, Germany, 2006.
(2) Dudney, N. J.; Neudecker, B. J. *Curr. Opin. Solid State Mater. Sci.* **1999**, *4*, 479−482.
(3) Sirisopanaporn, C.; Fernicola, A.; Scrosati, B. *J. Power Sources* **2009**, *186*, 490−495.
(4) Sakaebe, H.; Matsumoto, H. *Electrochem. Commun.* **2003**, *5*, 594−598.
(5) Matsumoto, H.; Sakaebe, H.; Tatsumi, K. *J. Power Sources* **2005**, *146*, 45−50.
(6) Garcia, B.; Lavallée, S.; Perron, G.; Michot, C.; Armand, M. *Electrochim. Acta* **2004**, *49*, 4583−4588.
(7) Shin, J. H.; Henderson, W. A.; Scaccia, S.; Prosini, P. P.; Passerini, S. *J. Power Sources* **2006**, *156*, 560−566.
(8) Fang, S.; Jin, Y.; Yang, L.; Hirano, S. I.; Tachibana, K.; Katayama, S. *Electrochim. Acta* **2011**, *56*, 4663−4671.
(9) Angenendt, K.; Johansson, P. *J. Phys. Chem. B* **2011**, *115*, 7808−7813.
(10) Liu, H.; Liu, Y.; Li, J. *Phys. Chem. Chem. Phys.* **2010**, *12*, 1685−1697.
(11) Barrosse-Antle, L. E.; Compton, R. G. *Chem. Commun.* **2009**, 3744−3746.
(12) Silvester, D. S.; Compton, R. G. *Z. Phys. Chem. (Muenchen)* **2006**, *220*, 1247−1274.
(13) Snuffin, L. L.; Whaley, L. W.; Yu, L. *J. Electrochem. Soc.* **2011**, *158*, F155−F158.
(14) Le, A. D.; Yu, L. *J. Electrochem. Soc.* **2011**, *158*, F10−F14.
(15) Andriola, A.; Singh, K.; Lewis, J.; Yu, L. *J. Phys. Chem. B* **2010**, *114*, 11709−11714.
(16) Chu, F.; Lin, B.; Yan, F.; Qiu, L.; Lu, J. *J. Power Sources* **2011**, *196*, 7979−7984.
(17) Lin, B.; Cheng, S.; Qiu, L.; Yan, F.; Shang, S.; Lu, J. *Chem. Mater.* **2010**, *22*, 1807−1813.

(18) Diao, H.; Yan, F.; Qiu, L.; Lu, J.; Lu, X.; Lin, B.; Li, Q.; Shang, S.; Liu, W.; Liu, J. *Macromolecules* **2010**, *43*, 6398−6405.
(19) Robertson, N. J.; Kostalik, H. A.; Clark, T. J.; Mutolo, P. F.; Abruña, H. c. D.; Coates, G. W. *J. Am. Chem. Soc.* **2010**, *132*, 3400−3404.
(20) Yan, F.; Yu, S.; Zhang, X.; Qiu, L.; Chu, F.; You, J.; Lu, J. *Chem. Mater.* **2009**, *21*, 1480−1484.
(21) Xiang, J.; Chen, R.; Wu, F.; Li, L.; Chen, S.; Zou, Q. *Electrochim. Acta* **2011**, *56*, 7503−7509.
(22) Yang, J.; Che, Q.; Zhou, L.; He, R.; Savinell, R. F. *Electrochim. Acta* **2011**, *56*, 5940−5946.
(23) Bai, Y.; Cao, Y.; Zhang, J.; Wang, M.; Li, R.; Wang, P.; Zakeeruddin, S. M.; Gratzel, M. *Nat. Mater.* **2008**, *7*, 626−630.
(24) Ito, S.; Zakeeruddin, S. M.; Comte, P.; Liska, P.; Kuang, D.; Gratzel, M. *Nat. Photonics* **2008**, *2*, 693−698.
(25) Kuang, D.; Klein, C.; Zhang, Z.; Ito, S.; Moser, J. E.; Zakeeruddin, S. M.; Grätzel, M. *Small* **2007**, *3*, 2094−2102.
(26) McIntosh, S.; Gorte, R. J. *Chem. Rev.* **2004**, *104*, 4845−4866.
(27) Whittingham, M. S.; Zawodzinski, T. *Chem. Rev.* **2004**, *104*, 4243−4244.
(28) Winter, M.; Brodd, R. J. *Chem. Rev.* **2004**, *104*, 4245−4270.
(29) Mehta, V.; Cooper, J. S. *J. Power Sources* **2003**, *114*, 32−53.
(30) Aricò, A. S.; Srinivasan, S.; Antonucci, V. *Fuel Cells* **2001**, *1*, 133−161.
(31) Li, Q.; He, R.; Jensen, J. O.; Bjerrum, N. J. *Chem. Mater.* **2003**, *15*, 4896−4915.
(32) Fuller, J.; Breda, A. C.; Carlin, R. T. *J. Electrochem. Soc.* **1997**, *144*, L67−L70.
(33) Greaves, T. L.; Drummond, C. J. *Chem. Rev.* **2007**, *108*, 206−237.
(34) Greaves, T. L.; Weerawardena, A.; Fong, C.; Krodkiewska, I.; Drummond, C. J. *J. Phys. Chem. B* **2006**, *110*, 22479−22487.
(35) Del Pópolo, M. G.; Kohanoff, J.; Lynden-Bell, R. M. *J. Phys. Chem. B* **2006**, *110*, 8798−8803.
(36) Yoshizawa, M.; Xu, W.; Angell, C. A. *J. Am. Chem. Soc.* **2003**, *125*, 15411−15419.
(37) Noda, A.; Susan, M. A. B. H.; Kudo, K.; Mitsushima, S.; Hayamizu, K.; Watanabe, M. *J. Phys. Chem. B* **2003**, *107*, 4024−4033.
(38) Blanchard, J. W.; Belières, J.-P.; Alam, T. M.; Yarger, J. L.; Holland, G. P. *J. Phys. Chem. Lett.* **2011**, *2*, 1077−1081.
(39) Yu, L.; Jin, X.; Zeng, X. *Langmuir* **2008**, *24*, 11631−11636.
(40) Jin, X.; Yu, L.; Garcia, D.; Ren, R. X.; Zeng, X. *Anal. Chem.* **2006**, *78*, 6980−6989.
(41) Umebayashi, Y.; Mori, S.; Fujii, K.; Tsuzuki, S.; Seki, S.; Hayamizu, K.; Ishiguro, S.-i. *J. Phys. Chem. B* **2010**, *114*, 6513−6521.
(42) Seki, S.; Ohno, Y.; Kobayashi, Y.; Miyashiro, H.; Usami, A.; Mita, Y.; Tokuda, H.; Watanabe, M.; Hayamizu, K.; Tsuzuki, S.; Hattori, M.; Terada, N. *J. Electrochem. Soc.* **2007**, *154*, A173−A177.
(43) Hayamizu, K.; Aihara, Y.; Nakagawa, H.; Nukuda, T.; Price, W. S. *J. Phys. Chem. B* **2004**, *108*, 19527−19532.
(44) Umecky, T.; Saito, Y.; Okumura, Y.; Maeda, S.; Sakai, T. *J. Phys. Chem. B* **2008**, *112*, 3357−3364.
(45) Kreuer, K. D.; Fuchs, A.; Ise, M.; Spaeth, M.; Maier, J. *Electrochim. Acta* **1998**, *43*, 1281−1288.
(46) Hardwick, L. J.; Holzapfel, M.; Wokaun, A.; Novak, P. *J. Raman Spectrosc.* **2007**, *38*, 110−112.
(47) Saito, Y.; Umecky, T.; Niwa, J.; Sakai, T.; Maeda, S. *J. Phys. Chem. B* **2007**, *111*, 11794−11802.
(48) Martinelli, A.; Matic, A.; Johansson, P.; Jacobssom, P.; Borjesson, L.; Fernicola, A.; Panero, S.; Scrosati, B.; Ohno, H. *J. Raman Spectrosc.* **2011**, *42*, 522−528.
(49) Gejji, S. P.; Suresh, C. H.; Babu, K.; Gadre, S. R. *J. Phys. Chem. A* **1999**, *103*, 7474−7480.